



# Compensation Temperature Behavior in a Nanotube Core-Shell Structure with RKKY Interactions: Monte Carlo Simulations

Z. Fadil<sup>1</sup>  · N. Maaouni<sup>1</sup> · A. Mhirech<sup>1</sup> · B. Kabouchi<sup>1</sup> · L. Bahmad<sup>1</sup> · W. Ousi Benomar<sup>1</sup>

Received: 13 July 2020 / Accepted: 16 September 2020 / Published online: 23 September 2020  
© Sociedade Brasileira de Física 2020

## Abstract

In this paper, we have studied the magnetic properties of the nanotube core-shell structure with RKKY (Ruderman-Kittel-Kasuya-Yosida) interactions, using Monte Carlo simulations (MCS). The system consists of hexagonal core-shell nanotube structure with mixed spins  $\sigma = \pm 3/2, \pm 1/2$  (of the core) and  $S = \pm 1, 0$  (of the shell), separated by non-magnetic nanotubes. Initially, we start this study by discussing for zero temperature, the ground-state phase diagrams in different planes. Moreover, we investigate for the positive temperature values, the effect of the RKKY interactions on the thermal magnetization and magnetic susceptibility of the system. Additionally, we study the effects of the exchange coupling interactions of the core and of the shell on the compensation and transition temperatures. Finally, we explore the behavior of the magnetic hysteresis cycles as a function of the non-magnetic nanotubes number, the temperature, and the exchange coupling parameters.

**Keywords** Nanotube core-shell structure · Magnetic properties · Compensation temperature · Transition temperature · Monte Carlo simulations · RKKY interactions · Magnetic hysteresis cycles

## 1 Introduction

The carbon element is located on the fourteenth column and the second period of the table of the elements [1, 2]. It therefore has six electrons, which can associate in three different ways called hybridizations. Only  $sp^2$  hybridizations and  $sp^3$  generate the forms of solid carbons allotropic. In the case of diamonds, carbon is  $sp^3$  hybridized and each atom is linked to four other atoms in a tetrahedral arrangement [3, 4]. The four bonds  $\sigma$  give the diamond its hardness, its transparency, and its property of electrical insulation [5]. Graphene has  $sp^2$  hybridization where each atom of carbon is linked to three other atoms in a planar pattern hexagonal [6]. In 1985, Smalley and his team highlight another allotropic form of carbon  $sp^2$  hybrid: the  $C_{60}$  fullerene or “bucky ball” [7]. These molecules, composed of 60 atoms of carbon, have the rounded shape of a football unlike graphite composed of planes. This new organization of carbon atoms gave rise to the idea that a tubular

structure was also possible. It was Iijima in 1991 who was credited with the first observation of this new object called carbon nanotube (CNTs) [8]. The CNTs can be single-walled carbon (SWCNT) nanotubes having diameters between 0.4 and 6 nm [9–11]. Their lengths range from a few hundred nanometers to several micrometers depending on the methods of synthesis. Or they can be multi-walled (MWCNT) comprising of several concentric interlinked nanotubes with space between each sheet 0.34 nm; their diameters can therefore reach several tens of nanometers [12–14]. In general, it is properly known that core-shell structure consists of a central particle (core) and a covering shell, which usually has different properties that the single component material does not have. The shell can change the surface charge density, functional groups, reactivity, biocompatibility, and stability of these composite structures [15–18]. In recent papers, the authors paid attention to the investigation of the magnetic properties using Monte Carlo simulations and relevant results were found such as the compensation temperature and the transition temperature between the ferrimagnetic and paramagnetic phases [19–31].

Moreover, the study of the magnetic properties of nanotubes is of great importance; several studies have been based on nanotubes such as the influence of temperature and electrodeposition potential on the magnetic properties of nickel

✉ Z. Fadil  
fadilzakaria604@gmail.com

<sup>1</sup> Laboratoire de Matière Condensée et Sciences Interdisciplinaires (LaMCScl), Faculty of Sciences, Mohammed V University, P.O.Box 1014, Rabat, Morocco

nanotube structure [32], the magnetic and electrical properties of carbon nanotube [33], and the magnetic properties of iron nanowire encapsulated in carbon nanotubes doped with copper [34]. In addition, the covalent atomic bridges enable a unidirectional enhancement of electronic transport in aligned carbon nanotubes [35], and we study RKKY (Ruderman-Kittel-Kasuya-Yosida) interaction in carbon nanotubes and graphene nanoribbons [36].

In this work, we study a system constituted by a magnetic nanotube core-shell structure, with mixed spins  $\sigma = \pm 3/2, \pm 1/2$  (of the core) and  $S = \pm 1, 0$  (of the shell), separated by a number of non-magnetic nanotubes ( $L$ ). The exchange coupling interactions RKKY (Ruderman-Kittel-Kasuya-Yosida) [37–41] is between the core and the shell atoms. The system is studied using Monte Carlo simulations (MCS) under the Metropolis algorithm. This paper is organized as follows: the model and method used are illustrated in Section 2, the ground-state phase diagrams are discussed in Section 3.1 and the Monte Carlo simulation (MCS) details in Section 3.2. Finally, the conclusion is given in Section 4.

## 2 Model and Method

The nanotube core-shell structure is studied in free boundary conditions frame. The system is composed with mixed spins  $\sigma = \pm 3/2, \pm 1/2$  (of the core) and  $S = \pm 1, 0$  (of the shell), separated by  $L$  number of non-magnetic nanotubes. The total number of the system spins is  $N = N_\sigma + N_S = 128$  with  $N_\sigma = 64$  and  $N_S = 64$  (see Fig. 1). In addition, we generate different configurations by sweeping sequentially the studied nanotube core-shell system making single-spin flips. Depending on the requirements of the Metropolis algorithm used, the spin flips are either accepted or rejected. The collected information was generated by  $5 \times 10^5$  configurations in the Monte Carlo simulations (MCS). Indeed to omit the initial conditions, we eliminate the first  $10^5$  iterations.

The Hamiltonian of the nanotube core-shell structure is given by:

$$\mathcal{H} = -J_S \sum_{\langle i,j \rangle} S_i S_j - J_c \sum_{\langle k,l \rangle} \sigma_k \sigma_l - J_{RKKY} \sum_{\langle m,n \rangle} S_m \sigma_n - H \sum_i (S_i + \sigma_i) - D_S \sum_i S_i^2 - D_\sigma \sum_j \sigma_j^2 \tag{1}$$

where  $J_S$  and  $J_c$  represent the exchange coupling interactions between the two first nearest neighbor atoms of the core and of the shell, respectively. The notations  $\langle i, j \rangle, \langle k, l \rangle$  and  $\langle m, n \rangle$  stand for the first near neighbor spins.  $J_{RKKY}$  means the interaction between the magnetic nanotube core-shell structures.  $H$  is the external magnetic field. The crystal fields called  $D_S$  and  $D_\sigma$  are acting on the spins  $S$  (of the shell) and  $\sigma$  (of the core), respectively. In all of this study, we will take the

identical crystal fields acting on the shell and on the core, respectively:  $D = D_S = D_\sigma$ .

The  $J_{RKKY}$  interaction, between the magnetic nanotube core-shell structures, is defined as follows:

$$J_{RKKY} = \frac{a^2 J_0}{L^2} \cos(K_f L) \tag{2}$$

The coefficient  $a$  represents the lattice constant,  $J_0$  is the magnetic coupling constant;  $K_f$  describes the Fermi level for a value of 0.5. Furthermore, the quantity  $a^2 J_0$  is equal to 1 as already taken in Refs. [42, 43].

The internal energy per site of the nanotube core-shell structure is defined by:

$$E = \frac{1}{N} \langle \mathcal{H} \rangle \tag{3}$$

The magnetizations of the shell and of the core and the total magnetization are given by:

$$M_S = \frac{1}{N_S} \sum_i S_i \tag{4}$$

$$M_\sigma = \frac{1}{N_\sigma} \sum_j \sigma_j \tag{5}$$

$$M_{tot} = \frac{M_S + M_\sigma}{2} \tag{6}$$

$N_\sigma$  and  $N_S$  are, respectively, the numbers of  $\sigma$  and  $S$  spins.

The partial and total magnetic susceptibilities are given by:

$$\chi_S = \beta (\langle M_S^2 \rangle - \langle M_S \rangle^2) \tag{7}$$

$$\chi_\sigma = \beta (\langle M_\sigma^2 \rangle - \langle M_\sigma \rangle^2) \tag{8}$$

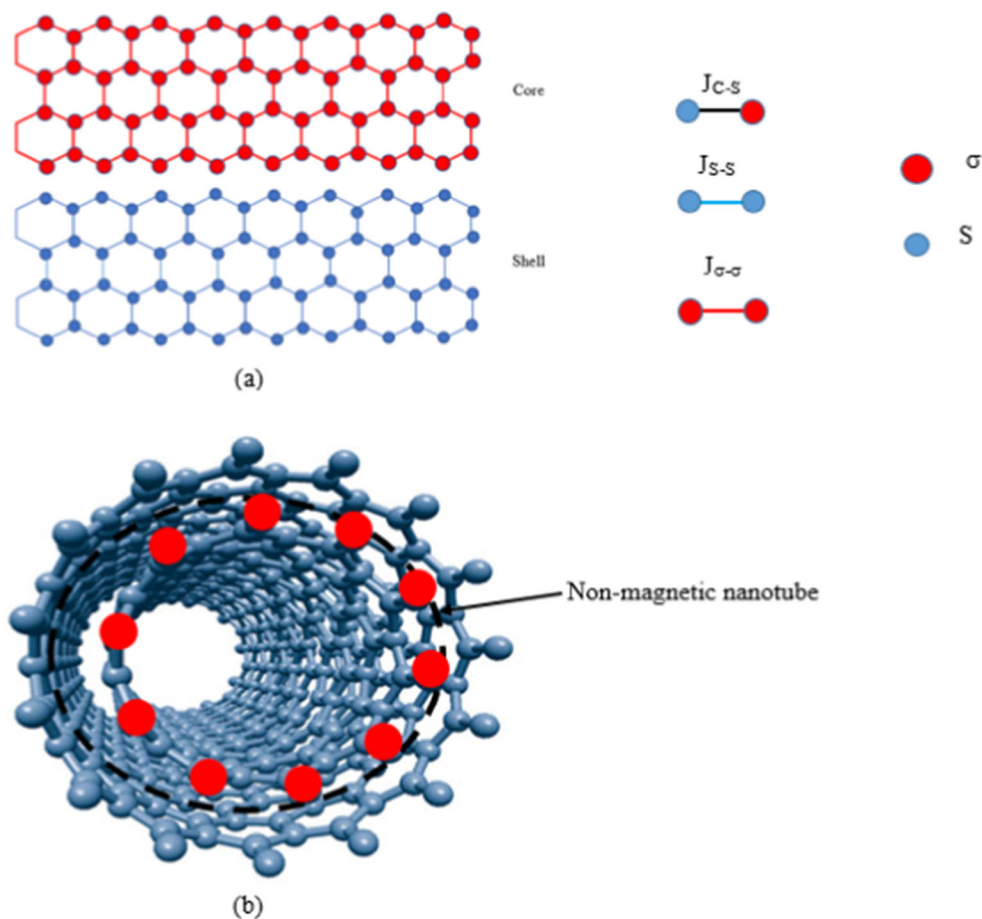
$$\chi_{tot} = \frac{\chi_S + \chi_\sigma}{2} \tag{9}$$

where  $\beta = \frac{1}{k_B T}$ ,  $k_B$  is the Boltzmann’s constant. It is supposed to take its unit value.  $T$  denotes the absolute temperature.

## 3 Numerical Results and Discussion

In the studied section, the results are obtained by using Monte Carlo simulations (MCS). Firstly, we investigate the ground-state phase diagrams for zero temperature value ( $T = 0$ ) in Section 3.1. Secondly, we explore in Section 3.2, for positive temperature values ( $T > 0$ ), the behavior of the thermal magnetizations and susceptibilities, the total magnetization as a function of the crystal field ( $D$ ), the exchange coupling interactions ( $J_C$  and  $J_S$ ), and the external magnetic field ( $H$ ).

**Fig. 1** A schematic representation in **a** two-dimensional and **b** three-dimensional of the magnetic nanotube core-shell structure separated by non-magnetic nanotubes



### 3.1 Ground-State Phase Diagrams ( $T = 0$ )

In this part, we study the ground-state phase diagrams based on the Hamiltonian of Eq. (1) governing the nanotube core-shell structure. For this purpose, we present in Fig. 2a–f the corresponding phase diagrams in the frame of the Blume-Capel model with mixed spins  $\sigma = \pm 3/2, \pm 1/2$  (of the core) and  $S = \pm 1, 0$  (of the shell). Such figures are plotted in different planes of several physical parameters. This model presents  $3 \times 4 = 12$  possible configurations. In fact, we opted in this work to the special case, where  $L = 1$ , to plot the ground-state phase diagrams.

Figure 2a shows the impact of the crystal and external magnetic fields on the stable configurations. For this end, we present the plane  $(H, D)$ , for fixed exchange coupling interactions of the core  $J_C = 1$  and of the shell  $J_S = 1$ . From this figure, we deduce that only six phases are stable from twelve possible configurations. These stable configurations are  $(+3/2, +1)$ ;  $(+1/2, +1)$ ;  $(+1/2, 0)$ ;  $(-1/2, 0)$ ;  $(-1/2, -1)$  and  $(-3/2, -1)$ . It is worth to note that these different stable configurations are appearing only for  $D < 0$ .

Moreover, in Fig. 2b is illustrated the plane  $(H, J_C)$ , in the absence of the crystal field ( $D = 0$ ) and for fixed exchange coupling interaction of the shell  $J_S = 1$ . It is found that only

four phases are stable, namely,  $(+1/2, +1)$ ;  $(+3/2, +1)$ ;  $(-1/2, -1)$  and  $(-3/2, 1)$ .

Besides, in Fig. 2c is plotted the plane  $(H, J_S)$ , in the absence of the crystal field ( $D = 0$ ) and for fixed exchange coupling interaction of the core,  $J_C = 1$ . This figure exhibits only four stable phases:  $(+3/2, 0)$ ;  $(+3/2, +1)$ ;  $(-3/2, 0)$  and  $(-3/2, -1)$ .

We notice that Fig. 2a–c exhibit a perfect symmetry regarding the external magnetic field axis  $H = 0$ .

In addition, to explore the effect of the exchange coupling parameter of the shell  $J_S$  and the crystal field  $D$ , we plot in Fig. 2d the plane  $(D, J_S)$ . This figure is illustrated in the absence of the external magnetic field ( $H = 0$ ) and fixed exchange coupling interaction of the core,  $J_C = 1$ . This figure exhibits six stable phases, namely,  $(+3/2, 0)$ ;  $(+3/2, +1)$ ;  $(-3/2, -1)$ ;  $(+1/2, 0)$ ;  $(-1/2, -1)$  and  $(+1/2, +1)$ .

To complete this study, we elucidate in Fig. 2e the stable configurations in the plane  $(D, J_C)$  in the absence of the external magnetic field ( $H = 0$ ). This figure is plotted for a fixed exchange coupling parameter value of the shell  $J_S = 1$ . Only six stable phases are present. We mention that the all-stable configurations found in this figure are those already found in Fig. 2d.

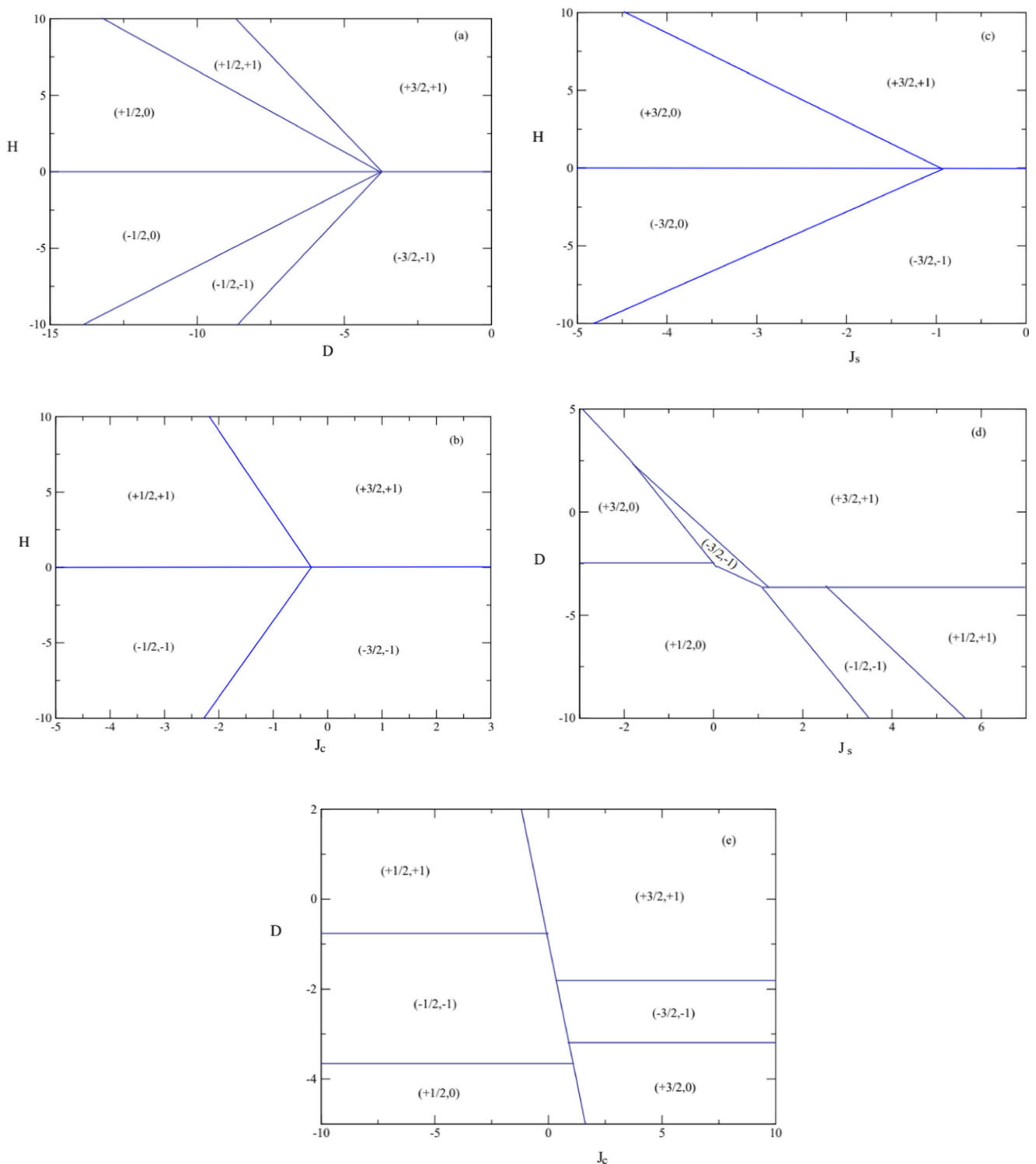


**Fig. 2** Ground-state phase diagrams for  $L = 1$ : **a** in the plane  $(H, D)$  for  $J_C = 1$  and  $J_S = 1$ ; **b**  $(H, J_C)$ ,  $J_S = 1$  and  $D = 0$ ; **c**  $(H, J_S)$ ,  $J_C = 1$  and  $D = 0$ ; **d**  $(D, J_S)$ ,  $J_C = 1$  and  $H = 0$ ; **e**  $(D, J_C)$ ,  $J_S = 1$  and  $H = 0$

### 3.2 Monte Carlo Simulations ( $T > 0$ )

In the present section, using Monte Carlo simulations (MCS) under the Metropolis algorithm, we study the  $J_{RKKY}$  interaction's effect on the magnetic properties of the nanotube core-

shell structure. In Fig. 3a, we present the behavior of the thermal partial ( $M_S$  and  $M_\sigma$ ) and total ( $M_{tot}$ ) magnetizations. Such figure is plotted in the absence of both parameter fields ( $H = 0$  and  $D = 0$ ) for fixed physical parameters of a number of non-magnetic nanotubes  $L = 5$  and exchange coupling of the core

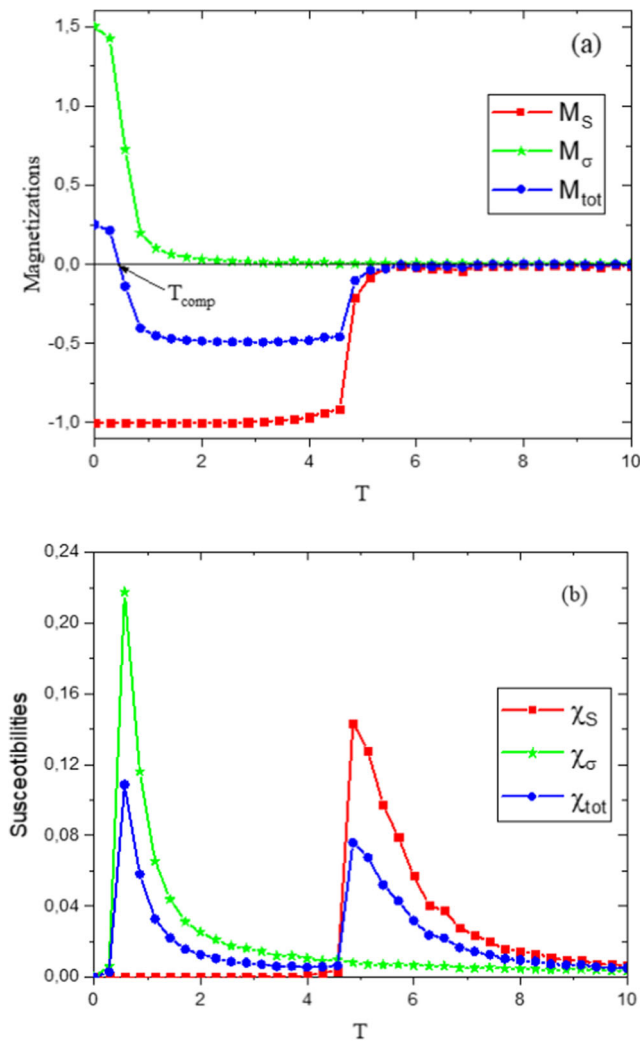


**Fig. 3** Thermal magnetizations (a) and susceptibilities (b) for fixed parameter values:  $D = 0$ ,  $H = 0$ ,  $L = 5$  and  $J_S = 2$  and  $J_C = 0.1$

$J_C = 2$  and exchange coupling of the shell  $J_S = 0.1$ . It is found that the total magnetization decreases towards a transition temperature  $T_r$ , corresponding to a zero total magnetization and the system tends towards the paramagnetic phase ( $M_{tot} \approx 0$ ). Moreover, the system exhibits a compensation temperature corresponding to zero total magnetization value. Indeed, this behavior is due to the competition between the exchange coupling interactions of the core and the shell. Such compensation temperature is located at the value  $T_{comp} \approx 0.5$  for selected parameters. Furthermore, we plot Fig. 3b for the same physical parameter values as in Fig. 3a. This figure presents the partials ( $\chi_S$ ,  $\chi_\sigma$ ) and total ( $\chi_{tot}$ ) magnetic susceptibilities. However, the total magnetic susceptibility shows two peaks. The first peak corresponds to the inflection point, while the second peak shows the location of the transition temperature ( $T_r \approx 4.86$ ). In fact,  $T_r$  indicates the transition between the ferrimagnetic ( $M_{tot} \neq 0$ ) and paramagnetic ( $M_{tot} = 0$ ) phases.

To inspect the effect of the non-magnetic nanotubes  $L$  on the behavior of the total magnetizations and susceptibilities,

we illustrate in Fig. 4a and b the obtained results. These figures are plotted for different numbers of intermediaries non-magnetic nanotubes ( $L = 1$ ,  $L = 2$  and  $L = 5$ ) in the absence of the crystal and external magnetic fields ( $D = 0$ ,  $H = 0$ ) and for fixed parameter values:  $J_S = 2$  and  $J_C = 0.1$ . Figure 4a shows that the compensation temperature ( $T_{comp}$ ) is found only for  $L = 5$  because the  $J_{RKKY}$  parameter is negative (ferrimagnetic parameter) while for  $L = 1$  and  $L = 2$  there is no compensation for the reason that the  $J_{RKKY}$  parameter is positive (ferromagnetic coupling). Furthermore, in Fig. 4b, the total magnetic susceptibility presents two peaks. The first one corresponds to the inflection point, while the second peak corresponds to the transition ( $T_r$ ) temperature. Indeed, it is found that the displacement of the magnetic susceptibility peaks towards the higher temperature values confirms the behavior of the total magnetization presented in Fig. 4a. The obtained compensation temperature value, for the non-magnetic nanotubes case  $L = 5$  is  $T_{comp} \approx 0.5$ . Besides, the obtained transition

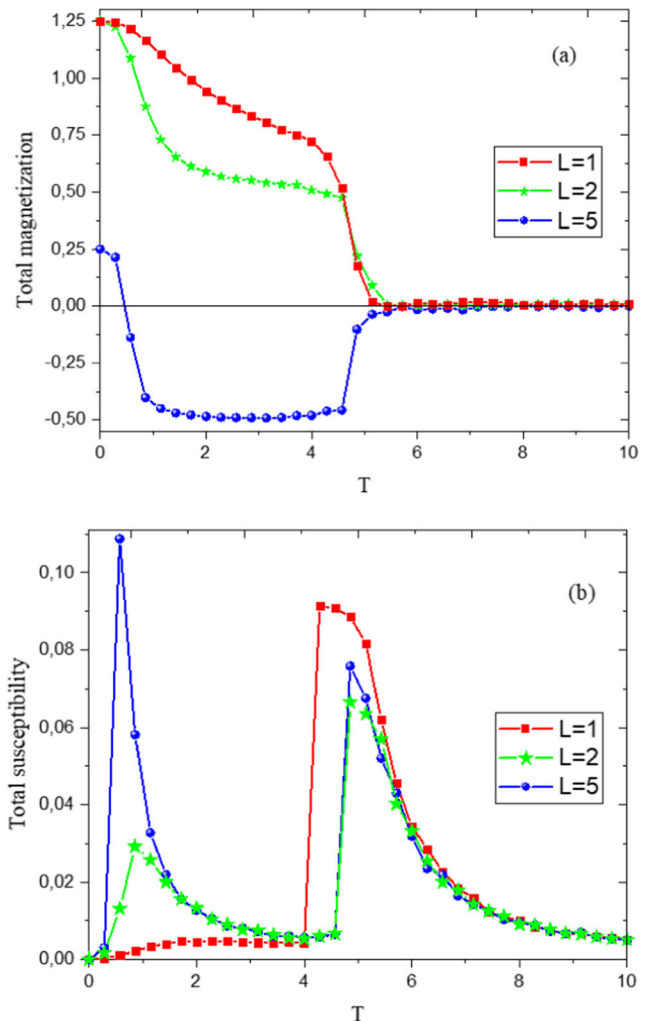


**Fig. 4** Thermal magnetizations (a) and susceptibilities (b) for fixed parameter values:  $D = 0$ ,  $H = 0$ ,  $J_S = 2$  and  $J_C = 0.1$

temperature for  $L = 1$  is  $T_r \approx 4.30$  while for  $L = 2$  and  $5$  is  $T_r \approx 4.86$ .

In order to study the effects of the exchange coupling interaction of the shell ( $J_S$ ), on the compensation and transition temperatures, we plot Fig. 5a and 5b for different values of the exchange coupling parameter of the shell ( $J_S = 1, 2, 3$ ), in the absence of the crystal and external magnetic fields ( $D = 0$  and  $H = 0$ ), for fixed parameter values of the number of non-magnetic nanotubes  $L = 5$  and for an exchange coupling interaction value of the core  $J_C = 0.1$ . It is found that the compensation temperature value is not affected by the variation of the exchange coupling interaction parameter  $J_S$ , whereas the transition temperature value increases when increasing the value of this parameter ( $J_S$ ). The obtained compensation temperature value ( $T_{comp}$ ), for all the selected values of the exchange coupling parameter  $J_S$  is  $T_{comp} \approx 0.5$ . Additionally, the obtained transition temperature for the parameter values  $J_S = 1, 2$  and  $3$  are  $T_r \approx 2.57, 4.86$  and  $7.43$ , respectively.

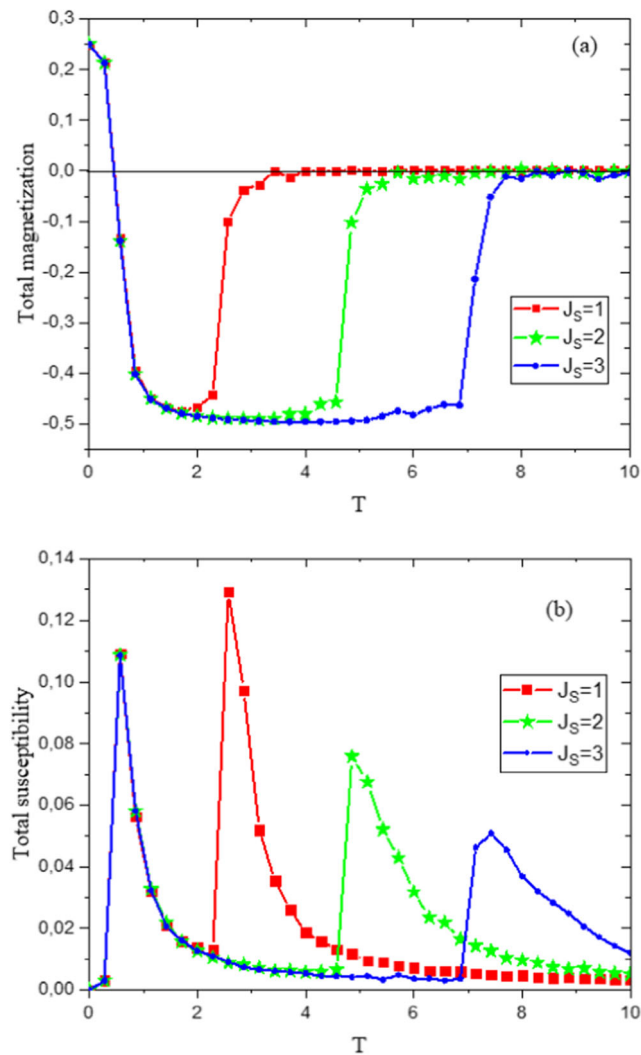


**Fig. 5** Thermal magnetizations (a) and susceptibilities (b) for fixed parameter values:  $D = 0, H = 0, L = 5$  and  $J_C = 0.1$

Following the same motivation, we evaluate Fig. 6a and b for different exchange coupling interaction values of the core ( $J_C = 0.1, 0.5, 0.7$  and  $1$ ) and for fixed parameter values:  $D = 0, H = 0, L = 5$  and  $J_S = 2$ . From this figure, we see that the compensation temperature ( $T_{comp}$ ) increases when increasing the value of the parameter  $J_C$ . On the other hand, the transition temperature value ( $T_r$ ) undergoes a decrease then increases for values of  $J_C$  greater than  $0.7$ . The obtained compensation temperature values for  $J_C = 0.1, 0.5, 0.7$ , and  $1$  are  $T_{comp} \approx 0.5, 2.2, 2.85$ , and  $4.55$ , respectively. Moreover, the obtained transition temperatures for the same values of the parameter  $J_C$  are  $T_r \approx 4.86, 4.28, 4.56$ , and  $5.14$ , respectively. It is also noted that when the value of  $J_C$  is further increased ( $J_C > 1$ ), the compensation temperature disappears.

In Fig. 7a, 7b, and 7c, we investigate the total magnetization ( $M_{tot}$ ) versus the crystal field ( $D$ ) and the exchange coupling interactions of the shell ( $J_S$ ) and of the core ( $J_C$ ), respectively. Such figures are plotted for several non-magnetic

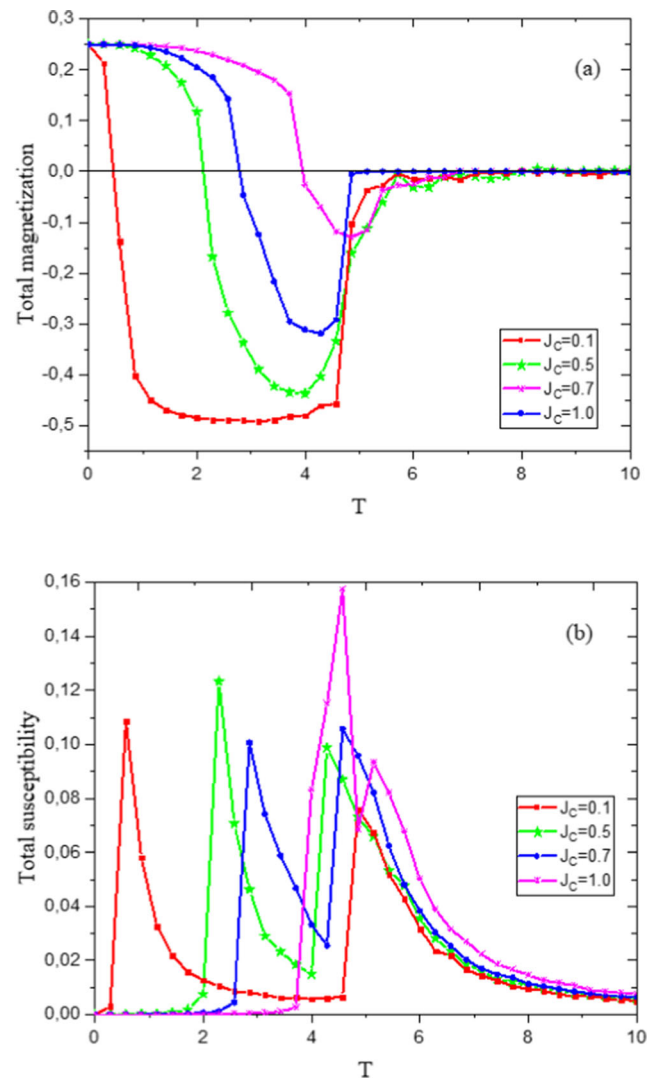


**Fig. 6** Thermal magnetizations (a) and susceptibilities (b) for fixed parameter values:  $D = 0, H = 0, L = 5$  and  $J_S = 2$

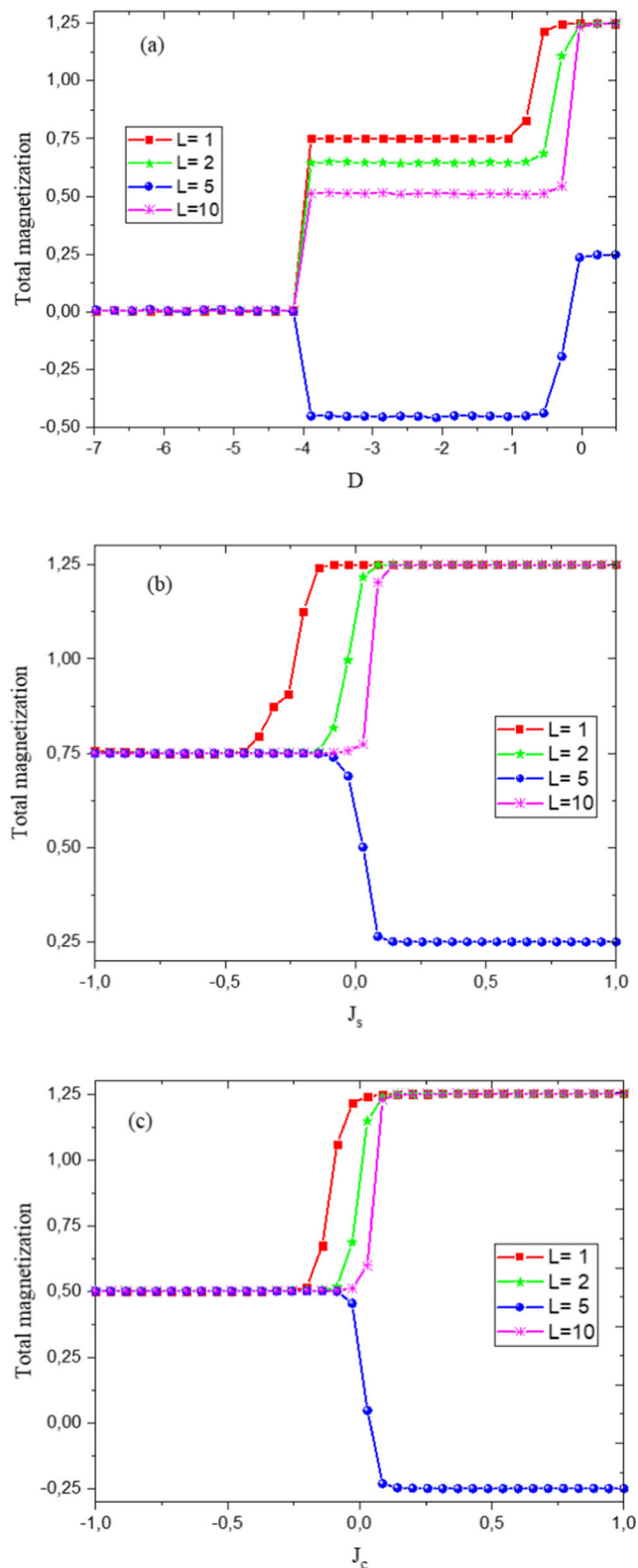


**Fig. 7** Total magnetization as a function of the crystal field, the exchange coupling interactions of the shell and of the core for  $H = 0$  and  $T = 0.2$ : **a**  $J_C = 0.1$  and  $J_S = 2$ , **b**  $J_C = 1$  and  $D = 0$ , **c**  $J_S = 1$  and  $D = 0$

nanotube values ( $L = 1, 2, 5$ , and  $10$ ), in the absence of the external magnetic field ( $H = 0$ ) and for fixed temperature

value  $T = 0.2$ . Figure 7a is obtained for fixed parameter values:  $J_C = 0.1$  and  $J_S = 2$ . From this figure, regardless of the non-magnetic nanotube values, the system shows three different regions: (i)  $D < -4.25$ , (ii)  $-4.25 < D < 0.5$ , and (iii)  $D > 0.5$ . In the region (i), the total magnetizations are kept constant and start with the value  $M_{tot} = 0.25$  ( $M_{tot} = \frac{3/2-1}{2}$ ) for  $L = 5$  because the parameter  $J_{RKKY}$  is negative and starts with the value  $M_{tot} = 1.25$  ( $M_{tot} = \frac{3/2+1}{2}$ ) for  $L = 1, 3$ , and  $10$ ; this is due to the positive value of  $J_{RKKY}$ . However, in the (ii), when increasing the parameter  $|D|$ , the total magnetization decreases and then increases for  $L = 5$ , while for  $L = 1, 3$ , and  $10$ , the total magnetization only decreases by undergoing a first-order transition. Finally, in the region (iii), the total magnetizations keep a constant value and the studied system reaches the paramagnetic phase ( $M_{tot} = 0$ ).

Moreover, we present in Fig. 7b the total magnetization versus the exchange coupling interaction of the shell ( $J_S$ ) for fixed parameter values:  $J_C = 1$  and  $D = 0$ . From this figure, whatever the non-magnetic nanotube values, the system shows three different states: (i)  $J_S > 0.2$ , (ii)  $-0.4 < J_S < 0.2$ , and (iii)  $J_S < -0.4$ . In the first state (i), the total magnetizations for large exchange coupling interaction values of the shell are kept constant and start with the value  $M_{tot} = 0.25$  for  $L = 5$  and start with the value  $M_{tot} = 1.25$  for  $L = 1, 3$  and  $10$ . Then, in the second state (ii), the total magnetization increase for  $L = 5$  by undergoing a second-order and decrease for  $L = 1, 3$ , and  $10$  by undergoing a first-order transition then remain constant. Finally, in the third state (iii), the total magnetization reaches the saturation value  $M_{sat} = 0.75$  more quickly when increasing the parameter  $L$ .

Besides, following the same motivation, we plot in Fig. 7c, the total magnetization as a function of the exchange coupling interaction of the core ( $J_C$ ), in the absence of the crystal field and for fixed parameter value:  $J_S = 1$ . In this figure, the system also presents three regions: (i)  $J_C > 0.2$ , (ii)  $-0.2 < J_C < 0.2$ , and (iii)  $J_C < -0.2$ . In the region (i), the total magnetizations for large exchange coupling interaction values of the core are kept constant and start with the value  $M_{tot} = -0.25$  ( $M_{tot} = \frac{-3/2+1}{2}$ ) for  $L = 5$  and  $M_{tot} = 1.25$  for  $L = 1, 2$ , and  $10$ . Furthermore, in the region (ii), the total magnetizations decreases (for  $L = 1, 2$  and  $10$ ) and increases (for  $L = 5$ ) following a second-order transition, due to the competition between different physical parameters of the nanotube system, then remain constant. Finally, in the region (iii), the total magnetization reaches the saturation value  $M_{sat} = 0.5$  more quickly when increasing the parameter  $L$ .

Finally, to complete this study, we examine in Fig. 8a–d the magnetic hysteresis cycle behavior of a nanotube core-shell structure in the absence of crystal field ( $D = 0$ ). These magnetic hysteresis cycles give the behavior of the total magnetization versus the external magnetic field ( $H$ ), highlighting the magnetic coercive field ( $H_C$ ), the saturation of the total

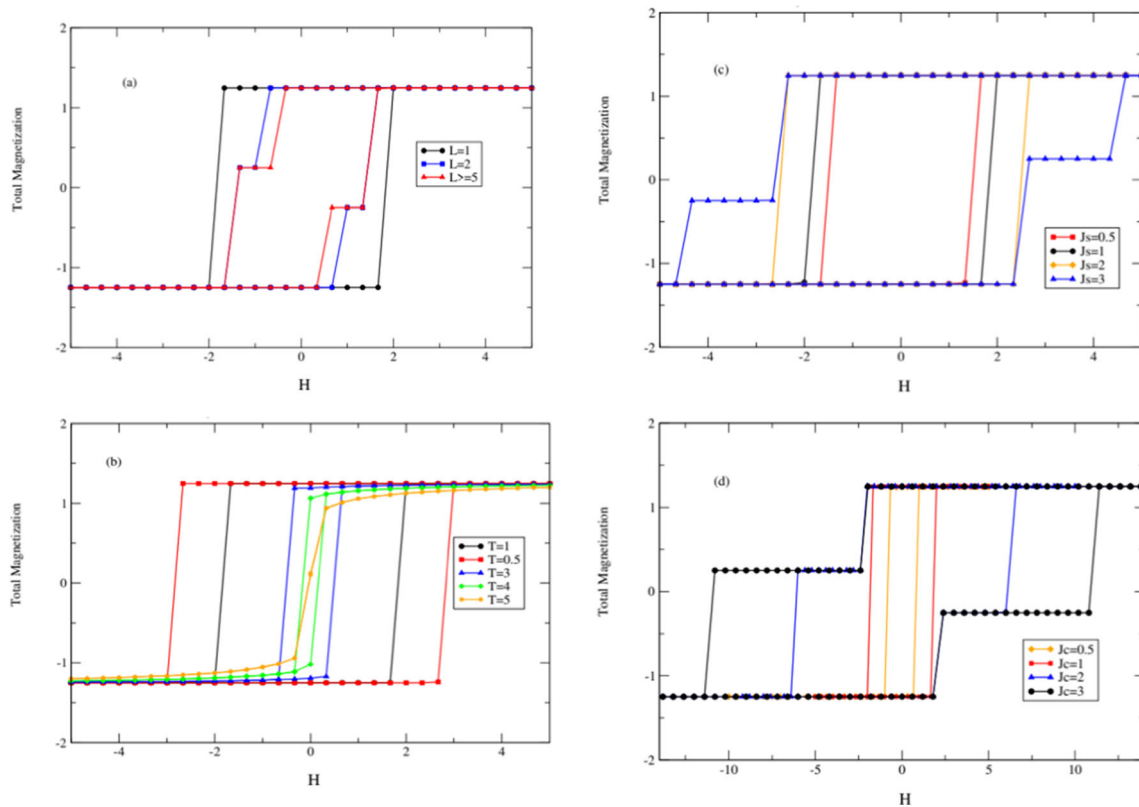


**Fig. 8** Magnetic hysteresis cycles of nanotube core-shell structure for  $D=0$ : **a**  $J_S = 1$ ,  $J_C = 1$ , and  $T = 1$ ; **b**  $J_S = 1$ ,  $J_C = 1$ , and  $L = 1$ ; **c**  $J_C = 1$ ,  $L = 1$ , and  $T = 1$ ; **d**  $J_S = 1$ ,  $L = 1$ , and  $T = 1$

magnetization, and the total remanent magnetization, and provide the information on the magnetic phases (ferrimagnetic or paramagnetic).

Figure 8a is plotted for different non-magnetic nanotube values  $L = 1, 2$ , and  $5$ , for fixed parameter values:  $J_S = 1$ ,  $J_C = 1$ , and  $T = 1$ . Such figure shows the decrease of the magnetic coercive field ( $H_C$ ) when increasing the number of non-magnetic nanotubes ( $L$ ) leading to a decrease in the surface loop. Therefore, for  $L \geq 5$ , the magnetic coercive field and the surface of the loop become constant.

Besides, Fig. 8b is plotted for selected values of temperature  $T = 0.5, 1, 3, 4$ , and  $5$ , for fixed parameter values:  $J_S = 1$ ,  $J_C = 1$  and  $L = 1$ . In this figure, the increase of the temperature parameter value decreases the magnetic coercive field leading to decreasing of the surface loop. The paramagnetic behavior is observed for  $T \geq 5$ .

Moreover, to explore the effect of the exchange coupling interaction of the shell ( $J_S$ ) on the magnetic hysteresis cycle, we plot Fig. 8c for different exchange coupling parameters of the shell,  $J_S = 0.5, 1, 2$ , and  $3$ . Such figure is established for fixed parameter values:  $J_C = 1$ ,  $L = 1$ , and  $T = 1$ . From this figure, the magnetic coercive field and the surface loop decreases when decreasing the parameter value  $J_S$ .

Finally, we investigate in Fig. 8d the effect of exchange coupling interaction of the core ( $J_C$ ) on the behavior of the hysteresis cycle. In this figure,  $J_C = 0.5, 1, 2$ , and  $3$ , for fixed

parameter values:  $J_S = 1$ ,  $L = 1$  and  $T = 1$ . From this figure, the same behavior of the magnetic coercive field and the surface loop in Fig. 8c is found.

### 4 Conclusion

In this work, we have studied the magnetic properties of the nanotube core-shell structure with mixed spins  $\sigma = 3/2$  (of the core) and  $S = 1$  (of the shell), with RKKY (Ruderman-Kittel-Kasuya-Yosida) interactions, using Monte Carlo simulations. The ground-state phase diagrams in different planes have been established. Moreover, we have investigated the effect of the RKKY interactions on the magnetization and the magnetic susceptibility of the system. It is found that the compensation temperature values decrease when increasing the number of the non-magnetic nanotubes ( $L$ ) and the exchange coupling interaction of the shell ( $J_S$ ), whereas the compensation temperature is not affected by the variation of the exchange coupling interaction of the core ( $J_C$ ). Besides, the total magnetization ( $M_{tot}$ ) versus the crystal field ( $D$ ), the exchange coupling interactions of the shell ( $J_S$ ) and of the core ( $J_C$ ), for several non-magnetic nanotubes values have been investigated. Finally, the magnetic hysteresis cycles are studied for fixed parameter values, namely,  $L, T, J_S$ , and  $J_C$ .



## References

- J.S. Gaffney, N.A. Marley, The Periodic Table of the Elements. General Chemistry for Engineers, 41 (2018)
- Q. Zhang, Z. Bai, F. Du, L. Dai, Carbon Nanotube Energy Applications. Nanotube Superfiber Materials, 695 (2019)
- L.W. Zhang, W.M. Ji, K.M. Liew, Mechanical properties of diamond nanothread reinforced polymer composites. Carbon **132**, 232–240 (2018)
- S. Pradeep, S. Surender, K. Prabhakaran, M. Jayasakthi, S. Singh, & al. Thin Solid Films, 649(2018) 12
- L. Chen, Understanding the thermal conductivity of diamond/copper composites by first-principles calculations. S. Chen and Y. Hou. Carbon **148**, 249–257 (2019)
- D. Akinwande, C.-J. Brennan, J. Scott Bunch, Philip Egberts, Jonathan R. Felts & al. Extreme Mechanics Letters, 13 (2017) 42, 77
- H.W. Kroto, J.R. Heath, S.C. O'Brien, R.F. Curl, R.E. Smalley, C60: Buckminsterfullerene. Nature **318**, 162–163 (1985)
- S. Iijima, Nature **354**, 56 (1991)
- N. Wang, Z.K. Tang, G.D. Li, J.S. Chen, Single-walled 4 Å carbon nanotube arrays. Nature **408**, 50–51 (2000)
- N.T. Alvarez, P. Miller, M.R. Haase, R. Lobo, R. Malik, V. Shanov, Tailoring physical properties of carbon nanotube threads during assembly. Carbon **144**, 55–62 (2019)
- P. Jittabut, S. Horpibulsuk, *Materialstodays: Proceedings*, vol 17 (2019), p. 1682
- I. Mustafa, I. Lopez, H. Younes, R.A. Susantyoko, R. Abu Al-Rub, S. Almheiri, Fabrication of freestanding sheets of multiwalled carbon nanotubes (Buckypapers) for vanadium redox flow batteries and effects of fabrication variables on electrochemical performance. Electrochimica Acta **230**, 222–235 (2017)
- E.M. Khabushev, D.V. Krasnikov, J.V. Kolodiaznaia, A.V. Bubis, A.G. Nasibulin, Structure-dependent performance of single-walled carbon nanotube films in transparent and conductive applications. Carbon **161**, 712–717 (2020)
- Y. Tian, M.Y. Timmermans, M. Partanen, A.G. Nasibulin, H. Jiang, Z. Zhu, E.I. Kauppinen, Growth of single-walled carbon nanotubes with controlled diameters and lengths by an aerosol method. Carbon **49**, 4636–4643 (2011)
- Z.Z. Lin, C.L. Huang, Z. Huang, W.K. Zhen, Applied Thermal Engineering **127**, 884 (2017)
- W. Wang, D.d. Chen, D. Lv, J.P. Liu, Q. Li, Z. Peng, Journal of Physics and Chemistry of Solids **108**, 39 (2017)
- F. Xu, S. Zhao, C. Lu, M. Potier-Ferry, Journal of the Mechanics and Physics of Solids **137**, 103892 (2020)
- W. Lu, X. Guo, Y. Luo, Q. Li, R. Zhu, H. Pang, Core-shell materials for advanced batteries. Chemical Engineering Journal **355**, 208–237 (2019)
- N. Maaouni, M. Qajjour, Z. Fadil, A. Mhirech, B. Kabouchi, L. Bahmad, W. Ousi Benomar, Magnetic and thermal properties of a core-shell borophene structure: Monte Carlo study. Physica B: Condensed Matter **566**, 63–70 (2019)
- A. Dakhama, N. Benayad, On the existence of compensation temperature in 2d mixed-spin Ising ferrimagnets: an exactly solvable model. Journal of Magnetism and Magnetic Materials **213**, 117–125 (2000)
- Z. Fadil, A. Mhirech, B. Kabouchi, L. Bahmad, W. Ousi Benomar, Superlattices and Microstructures **135**, 106285 (2019)
- Z. Fadil, A. Mhirech, B. Kabouchi, L. Bahmad, W.O. Benomar, Magnetization and compensation behaviors in a mixed spins (7/2, 1) anti-ferrimagnetic ovalene nano-structure. Superlattices and Microstructures **134**, 106224 (2019)
- M. Qajjour, N. Maaouni, Z. Fadil, A. Mhirech, B. Kabouchi, W. Ousi Benomar, L. Bahmad, Dilution effect on the compensation temperature in a honeycomb nano-lattice: Monte Carlo study. Chinese Journal of Physics **63**, 36–44 (2020)
- Z. Fadil, M. Qajjour, A. Mhirech, B. Kabouchi, L. Bahmad, W. Ousi Benomar, Dilution effects on compensation temperature in nano-trilayer graphene structure: Monte Carlo study. Physica B: Condensed Matter **564**, 104–113 (2019)
- J.P. Santos, F.C. Sá Barreto, An effective-field theory study of trilayer Ising nanostructure: Thermodynamic and magnetic properties. Journal of Magnetism and Magnetic Materials **439**, 114–119 (2017)
- Z. Fadil, M. Qajjour, A. Mhirech, B. Kabouchi, L. Bahmad, W. Ousi Benomar, Magnetization and susceptibility behaviors in a bi-layer graphyne structure: A Monte Carlo study. Physica B: Condensed Matter **578**, 411852 (2020)
- Y. Nakamura, Existence of a compensation temperature of a mixed spin-2 and spin-5/2 Ising ferrimagnetic system on a layered honeycomb lattice. Physical Review B **62**, 11742–11746 (2000)
- B. Boechat, R. Filgueiras, L. Marins, C. Cordeiro, N.S. Branco, FERRIMAGNETISM IN TWO-DIMENSIONAL MIXED-SPIN ISING MODEL. Modern Physics Letters B **14**, 749–758 (2000)
- B. Boechat, R.A. Filgueiras, C. Cordeiro, N.S. Branco, Renormalization-group magnetization of a ferrimagnetic Ising system. Physica A: Statistical Mechanics and its Applications **304**, 429–442 (2002)
- M. Godoy, V.S. Leite, W. Figueiredo, Mixed-spin Ising model and compensation temperature. Physical Review B **69**, 054428 (2004)
- Z. Fadil, A. Mhirech, B. Kabouchi, L. Bahmad, W. Ousi Benomar, Polarization and dielectric susceptibility of a monolayer coronene like nano-structure: Monte Carlo study. Physics Letters A **384**, 126783 (2020)
- G. Kalkabay, A. Kozlovskiy, M. Zdorovets, D. Borgekov, E. Kaniukov, A. Shumskaya, Influence of temperature and electrodeposition potential on structure and magnetic properties of nickel nanotubes. Journal of Magnetism and Magnetic Materials **489**, 165436 (2019)
- I. Pelech, R. Pelech, U. Narkiewicz, A. Kaczmarek, N. Guskos, G. Żolnierkiewicz, J. Typekc, P. Berczyński, Materials Science and Engineering B **254**, 114507 (2020)
- C. Wu, K.L. Shi, Y. Zhang, W. Jiang, Magnetic properties of iron nanowire encapsulated in carbon nanotubes doped with copper. Journal of Magnetism and Magnetic Materials **465**, 114–121 (2018)
- M. Chen, W. Li, A. Kumar, G. Li, M.E. Itkis, B.M. Wong, E. Bekyarova, ACS Applied Materials & Interfaces **11**, 19315 (2019)
- J. Klinovaja, D. Loss, RKKY interaction in carbon nanotubes and graphene nanoribbons. Physical Review B **87**, 045422 (2013)
- M. Zare, F. Parhizgar, R. Asgari, Strongly anisotropic RKKY interaction in monolayer black phosphorus. Journal of Magnetism and Magnetic Materials **456**, 307–315 (2018)
- Z. Fadil, M. Qajjour, A. Mhirech, B. Kabouchi, L. Bahmad, W. Ousi Benomar, Blume-Capel model of a bi-layer graphyne structure with RKKY Interactions: Monte Carlo simulations. Journal of Magnetism and Magnetic Materials **491**, 165559 (2019)
- Z. Fadil, A. Mhirech, B. Kabouchi, L. Bahmad, W. Ousi Benomar, Magnetic properties of naphthalene-like nano-structure with RKKY interactions: Monte Carlo simulations. Chinese Journal of Physics **64**, 295–304 (2020)
- T. Balcerzak, K. Szałowski, M. Jaščur, Thermodynamic model of a solid with RKKY interaction and magnetoelastic coupling. Journal of Magnetism and Magnetic Materials **452**, 360–372 (2018)
- T. Balcerzak, J.W. Tucker, Journal of Magnetism and Magnetic Materials **278**, 87 (2004)
- T. Kasuya, A theory of metallic ferro- and antiferromagnetism on Zener's model. Progress in Theoretical Physics **16**, 45–57 (1956)
- K. Yosida, Magnetic Properties of Cu-Mn Alloys. Physics Review **106**, 893–898 (1957)

**Publisher's Note** Springer Nature remains neutral with regard to jurisdictional claims in published maps and institutional affiliations.